S1. Experimental Section

Materials. Cobalt (II) chloride ($CoCl_2$, ≥98.0%), 2-methylimidazole (MeIm, 99%), polyvinylpyrrolidone K30 (PVP, ≥99.5%), and L-glutamic acid (LGA, ≥99%) were purchased from Sigma-Aldrich. 1,3,5-triformylphloroglucinol (TFP, >98.0%) and 2,5-dimethyl-*p*-phenylenediamine (DMPA, >97.0%) were obtained from Tokyo Chemical Industry. Acetic acid (HAc, ≥99.0%), methanol (>99.8%), ethanol (≥99.5%), isopropanol (≥99.7%), and *N*, *N*-dimethylformamide (DMF, >99.5%) were purchased from FUJIFILM Wako Pure Chemical Corporation. All chemicals were used directly without further purification.

Synthesis of ZIF-67 and etched ZIF-67. In a typical synthesis of ZIF-67, 259.7 mg of $CoCl_2$ (2.0 mmol) was ultrasonically dissolved in methanol (30 mL), and 10 mL of PVP (30 mg mL^{-1}) methanolic solution was subsequently added to the Co^{2+} solution and stirred for 10 min. Then, 1.314 g of MeIm (16.0 mmol) was completely dissolved in methanol (20 mL) to form another clear solution. The two methanolic solutions were mixed together and vigorously shaken for 5 min. The mixture solutions were then aged at room temperature for 12 h. After that, the purple ZIF-67 precipitate was collected, separated by centrifugation, washed carefully with methanol, and dried at 60 °C overnight.

For the construction of etched ZIF-67, a simple wet-chemistry process[S1] at room temperature was adopted. In a typical operation, 20 mg of the as-prepared ZIF-67 polyhedrons were ultrasonically dispersed in 60 mL of methanol for 15 min. Next, 20 mL of LGA etchant solution was subsequently injected into the ZIF-67 solution, and the resulting mixture was stirred for 8 h. The etched ZIF-67 polyhedrons were collected by centrifugation and washed with water and methanol.

Carbonization of etched ZIF-67 derived graphitic carbon. The etched ZIF-67 polyhedrons were pyrolyzed with a heating rate of 2 °C min^{-1} under nitrogen gas flow from room temperature to 800 °C and maintained at 800 °C for 3 h. After cooling to ambient temperature, the annealed product was then dispersed in 0.5 M H_2SO_4 solution for 8 h at 80 °C to remove the deposited Co species. The etched ZIF-67-derived graphitic carbon (MOF-GC) was harvested by several rinse-centrifugation cycles with deionized water and ethanol until the

supernatant became neutral, and then dried under vacuum at 60 °C overnight.

Synthesis of MOF-GC@COF heterostructure. In a typical synthesis of MOF-GC@COF-TFP-DMPA, 20 mg of the as-prepared MOF-GC particles were ultrasonically dispersed in 20 mL of ethanol for 1 h to obtain a homogeneous solution. Following this, 20 mL of DMPA monomer (0.015 mM, DMF) was added to the aforementioned solution with stable stirring for 10 min, 20 mL of TFP monomer (0.01 mM, DMF) and 3 mL HAc (6 M) was subsequently added into the above solution and further stirring for 30 min. After that, the mixture solution was heated at 90 °C for 24 h to assemble COF-TFP-DMPA onto the MOF-GC templates. The resulting precipitate, MOF-GC@COF heterostructure with a core-shell structure, was finally collected *via* centrifugation and washed with DMF and ethanol for three times, respectively, and dried in vacuum overnight. The thickness of the COF shell in the MOF-GC@COF heterostructure could be tuned by changing the concentration ratio of the COF monomer to the MOF-GC core. The MOF-GC@COF-TFP-DMPA heterostructure is noted as MOF-GC@COF_x, where x indicates the concentration of TFP monomer in the product.

Characterization. The morphology of the as-synthesized materials was observed on a field emission scanning electron microscope (FESEM, Hitachi SU-8000) with an accelerating voltage of 10.0 kV. Transmission electron microscopy (TEM), scanning transmission electron microscopy (STEM) images, energy-dispersive X-ray spectroscopy (EDXS), and elemental mapping analysis were performed using a JEM-2100F (JEOL, Japan) operated at 200 kV. Wide-angle X-ray diffraction (XRD) patterns were obtained by using a Rigaku Rint 2000 X-ray diffractometer with monochromatic Cu Kα radiation (40 kV, 40 mA) at a scan rate of 2 °C min^{-1}. The nitrogen adsorption-desorption isotherms were obtained by using a Quantachrome Autosorb-iQ Automated Gas Sorption System at 77 K and the specific surface area was evaluated by the multipoint Brunauer-Emmett-Teller (BET) method.

QCM sensing of formaldehyde. The 9 MHz AT-cut crystal electrodes coated with the MOF-GC@COF_x heterostructures were assembled in a QCM instrument (QCA922, SEIKO, Japan) for the determination of

frequency changes induced by the adsorbed mass. Before coating the QCM electrode with the heterostructure, the blank gold (Au) electrode was initially ultrasonicated in a mixture solution of ethanol and water (1: 1, *v/v*) for 30 min and then dried under nitrogen flow. After that, the frequency of the blank electrode was recorded as a fundamental frequency (f_0). A homogeneous precursor solution was prepared by ultrasonic dispersion of 1.0 mg mL^{-1} MOF-GC@COF$_x$ in ethanol for 30 min, which was then directly coated onto the both sides of the Au electrode *via* a simple drop-coating method based on our previous studies.[S2] The MOF-GC@COF$_x$ coated QCM electrode was dried under a gentle stream of nitrogen, before being dried in vacuum for another 2 h. The frequency of the heterostructure-coated QCM electrode was recorded when a stable baseline (±2 Hz min^{-1}) appeared and the frequency values were used to estimate the mass of the prepared QCM electrode by using the Sauerbrey equation.[S2] All QCM measurements were performed at room temperature in a sealed 300 mL chamber and the time dependence of frequency shift (Δf) was monitored during sequential injections of chemical vapors, *e.g.*, formaldehyde (HCHO), formic acid (HCOOH), water (H_2O), ammonia (NH_3), triethylamine (Et_3N), methanol (MeOH), ethanol (EtOH), and *n*-hexane (C_6H_{12}).

S2. Adsorption kinetics

To investigate the adsorption kinetics of the MOF-GC@COF heterostructure toward HCHO, the pseudo-first-order model and pseudo-second-order model were used to fit the QCM experimental data.[S3] For the pseudo-first-order kinetics, the concentration of adsorbed HCHO on the surface of the MOF-GC@COF was assumed to be always constant and the diffusion was controlled by the concentration gradient through the heterostructure. The rates of vapor uptake ($\Delta f_t/\Delta f_\infty$) can be calculated in terms of the pseudo-first-order rate constant (k_1) as expressed by Equations (1) and (2):[S3]

$$\frac{\Delta f_t}{\Delta f_\infty} = 1 - e^{-k_1 t} \quad (1)$$

$$-ln\left(1 - \frac{\Delta f_t}{\Delta f_\infty}\right) = k_1 t \quad (2)$$

where Δf_t and Δf_∞ refer to the frequency changes of formaldehyde at time t and at equilibrium state, respectively. The plot of $-ln(1-\Delta f_t/\Delta f_\infty)$ against time t is a linear regression equation with a slope of k_1.

The pseudo-second-order rate reaction is dependent on the amount of formaldehyde adsorbed on the surface of the adsorbent and the amount adsorbed at equilibrium. It can be represented by Equations (3) and (4) as shown below:[S3]

$$\frac{t}{\Delta f_t} = \frac{1}{k_2 \Delta f_\infty} + \frac{t}{\Delta f_\infty} \tag{3}$$

$$\frac{\Delta f_t}{\left(\Delta f_\infty - \Delta f_t\right)\Delta f_\infty} = k_2 t \tag{4}$$

Since the frequency shifts of the QCM sensing are negative numbers, here, Δf_t and Δf_∞ refer to the absolute values of the frequency changes at time t and at equilibrium state, respectively. The plot of $\Delta f_t/[(\Delta f_\infty-\Delta f_t)\Delta f_\infty]$ against time t is a linear regression equation with a slope of k_2 of pseudo-second-order model.

Table S1. Summary of the pseudo-first-order model and pseudo-second-order model for the QCM sensing of formaldehyde vapor by the MOF-GC@$COF_{0.002}$, MOF-GC@$COF_{0.01}$, MOF-GC@$COF_{0.05}$, pristine MOF-GC, and pristine COF-based sensors.

QCM materials	**Pseudo-first-order model**		**Pseudo-second-order model**	
	k_1 (min^{-1})	r^2	k_2 (Hz^{-1} min^{-1})	r^2
MOF-GC@$COF_{0.002}$	1.436	0.9984	0.046	0.9104
MOF-GC@$COF_{0.01}$	1.026	0.9975	0.024	0.9289
MOF-GC@$COF_{0.05}$	0.805	0.9917	0.017	0.9770
Pristine MOF-GC	1.759	0.9912	0.065	0.9737
Pristine COF	0.709	0.9892	0.012	0.9844

Table S2. Brief summary of formaldehyde sensing performance of various QCM sensors based on -NH_2 group-containing nanostructures at room temperature.

Sensing materials [a]	**Surface area (m^2 g^{-1})**	**Fabrication method**	**Frequency shift (HCHO concentration)**	**Reference**
PEI/PVA	-	Electrospinning	124 Hz (255 ppm)	[S4]
PEI/PS	47.25	Electrospinning	75 Hz (140 ppm)	[S5]
PEI/BC	-	Drop-coating	152.8 Hz (100 ppm)	[S6]
PEI-PA 6 NFN	19.77-31.23	Electrospinning/netting	22 Hz (20 ppm)	[S7]
PEI-TiO_2	68.72	Drop-coating	13.7 Hz (100 ppm)	[S8]
PAN-PVAm	25	Drop-coating	4.2 Hz (15 ppm)	[S9]
Copper (II) functional complex	-	PVD and *in-situ* growth[b]	500 Hz (20 ppm)	[S10]
PDA nanotubes	30.0-52.1	Drop-coating	1328 Hz (50 ppm)	[S11]
PODS-PDA	-	Self-assembly	229 Hz (30 ppm)	[S12]
PDA/HMSSs	686-955	Drop-coating	687 Hz (10 ppm)	[S13]
DDS urea dry-gel	-	Drop-coating	334 Hz (50 ppm)	[S14]
Amine-functionalized SBA-15	218-482	Sol-gel	745 Hz (50 ppm)	[S15]
MOF-GC@COF	437-510	Drop-coating	151.8 Hz (1 ppm)	This study

[a] PEI-PA 6 NFN: polyethyleneimine (PEI) functionalized polyamide 6 nano-fiber/net; PEI/PVA: polyethyleneimine/poly(vinyl alcohol); PEI/PS: polyethyleneimine/polystyrene; PEI/BC: polyethyleneimine/ bacterial cellulose; PEI-TiO_2: polyethyleneimine functionalized TiO_2 nanofiber; Copper (II) functional complex: $[Cu(DDS)_2(Cl)_2(MeOH)_2]$; PDA nanotubes: polydopamine nanotubes; PODS-PDA: polymerized *n*-octadecylsiloxane and polydopamine; PDA/HMSSs: polydopamine-functionalized hollow mesoporous silica spheres; DDS urea dry-gel: diamino diphenyl sulfone urea dry-gel; Amine-functionalized SBA-15: amine groups functionalized on the inner wall of uniform hexagonal lamelliform mesoporous SBA-15.

b PVD and *in-situ* growth: The physical vapor deposition (PVD) method is used for coating a thin layer of copper on the surface of QCM silver electrode. And then, copper (II) functional complex is grown *in-situ* on the copper layer.

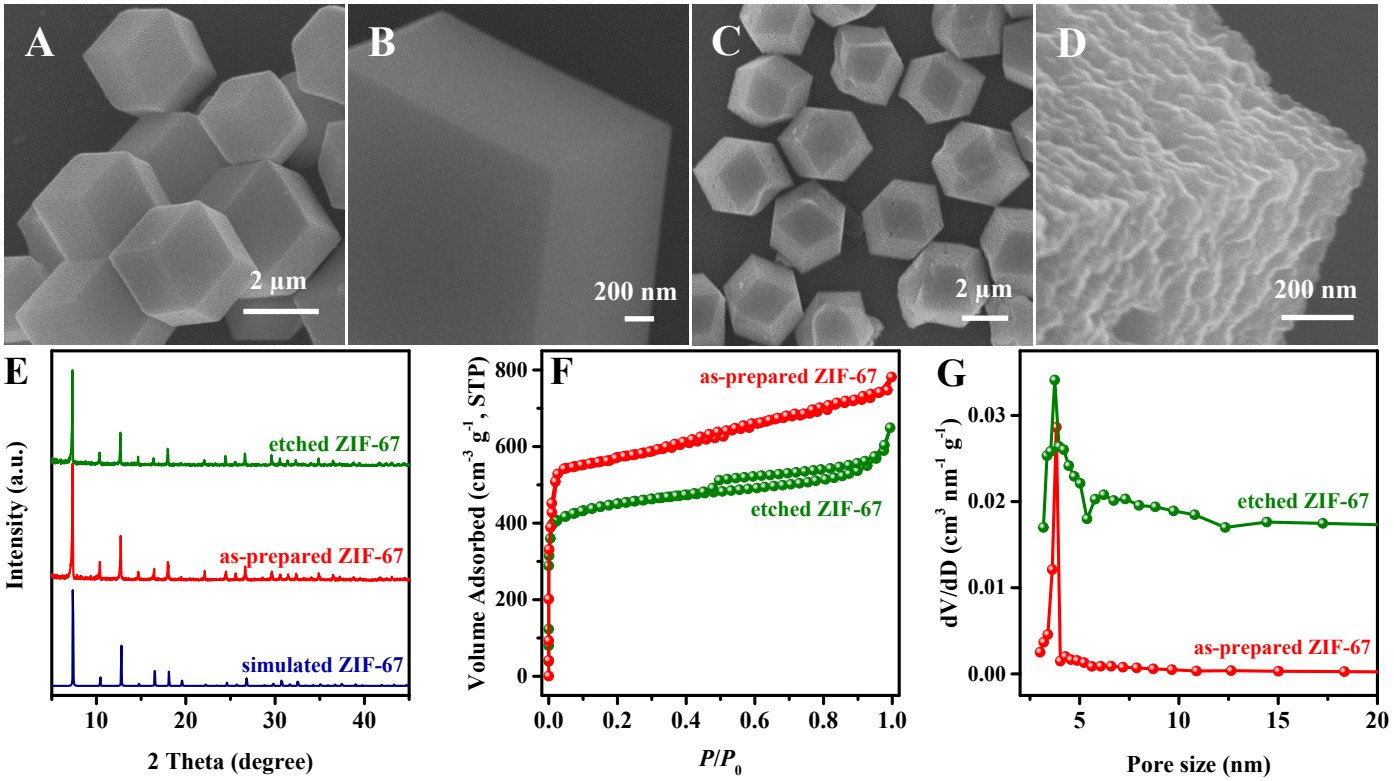

Fig. S1. SEM images of as-prepared ZIF-67 crystals before (A, B) and after (C, D) etching with L-glutamic acid. (D) XRD patterns of simulated ZIF-67, as-prepared ZIF-67 crystals, and etched ZIF-67 crystals. (F) Nitrogen adsorption-desorption isotherms and (G) pore size distribution curves of as-prepared ZIF-67 and etched ZIF-67 crystals.

Note for Fig. S1. The porosity of the etched ZIF-67 crystals was investigated by N_2 adsorption-desorption measurements (**Fig. S1F**). A steady N_2 adsorption is observed at a low relative pressure, suggesting that the etching process does not destroy the microporosity of ZIF-67. Interestingly, the N_2 adsorption-desorption isotherms of the etched ZIF-67 sample also show a hysteresis loop at a high relative pressure, unlike the pristine ZIF-67, suggesting the generation of mesoporosity after chemical etching. Pore size analysis confirms the existence of mesopores, as shown in **Fig. S1G**.

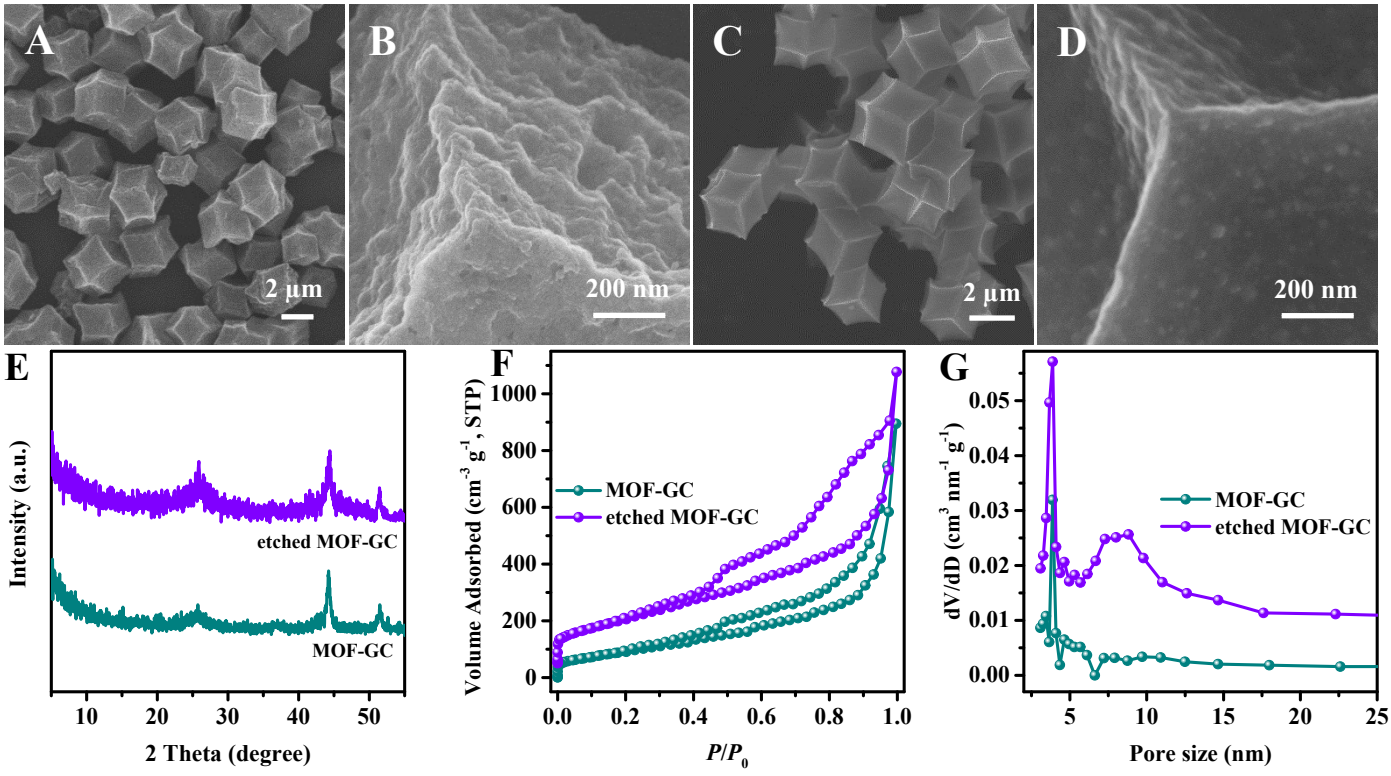

Fig. S2. SEM images of graphitic carbon derived from etched ZIF-67 (etched MOF-GC, A, B) and pristine (unetched) ZIF-67 (MOF-GC, C, D). (E) XRD patterns of etched MOF-GC and pristine MOF-GC. (F) Nitrogen adsorption-desorption isotherms and (G) pore size distribution curves of etched MOF-GC and pristine MOF-GC.

Note for Fig. S2. In a typical synthesis of MOF-GC, the pristine ZIF-67 precursor was directly converted to MOF-GC through carbonization under N_2 flow at 800 °C for 3 h, with a heating rate of 2 °C·min^{-1} (**Fig. S2C**, **D**). The PXRD patterns of both etched and unetched MOF-GC display a diffraction peak at ~26°, which can be indexed to the (002) diffraction of graphitic carbon structure (**Fig. S2E**). The other intense peaks located at around 44° and 51° are indexed to the (111) and (200) peaks of face-centered-cubic (*fcc*) Co crystal (**Fig. S2E**). The BET surface areas of etched MOF-GC and unetched MOF-GC are 437, and 524 m^2 g^{-1} (**Fig. S2F**), respectively. Pore size analysis confirms the generation of mesopores in the etched MOF-GC sample (**Fig. S2G**).

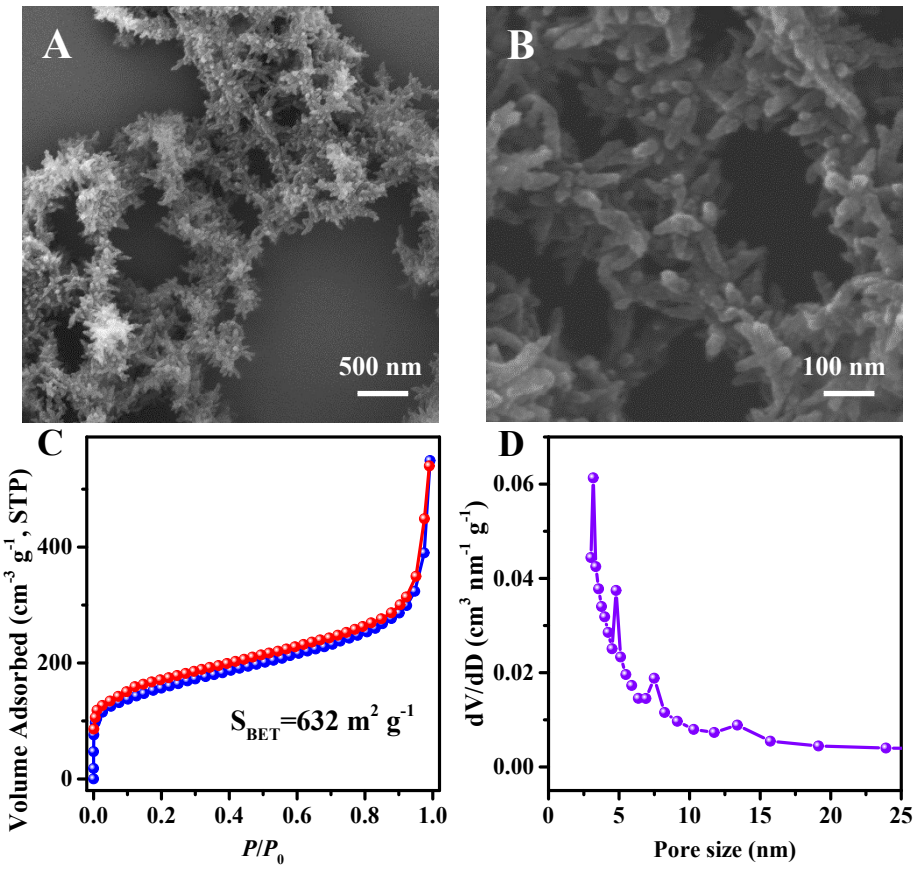

Fig. S3. SEM images (A, B), nitrogen adsorption-desorption isotherms (C) and pore size distribution curve (D) of pure COF-TFP-DMPA.

Note for Fig. S3. In a typical synthesis of pure COF-TFP-DMPA, 20 mL of DMPA monomer (0.03 mM, DMF) was added to the DMF solution of TFP monomer (0.02 mM, 20 mL), followed by the addition of 3 mL HAc (6 M) and subsequent stirring for 30 min. After that, the mixture solution was heated at 90 °C for 24 h to promote the growth of pure COF-TFP-DMPA.

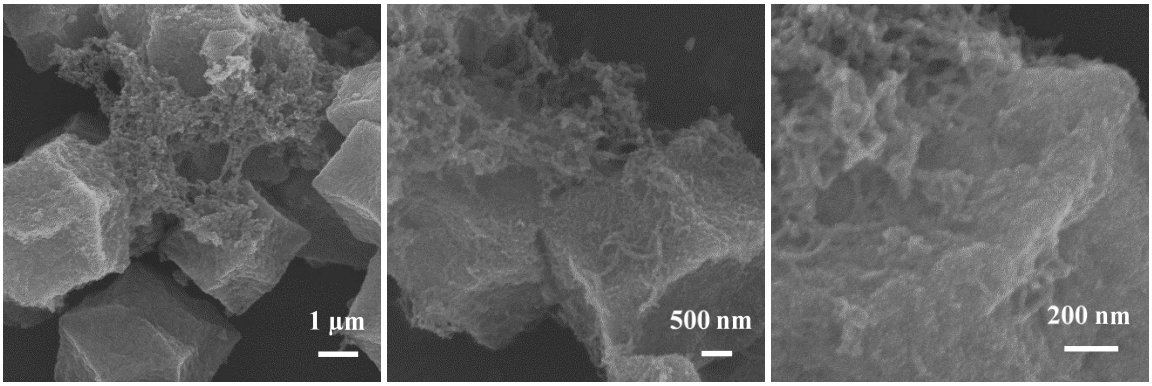

Fig. S4. SEM images of the hybrid material obtained directly using MOF-GC without surface etching.

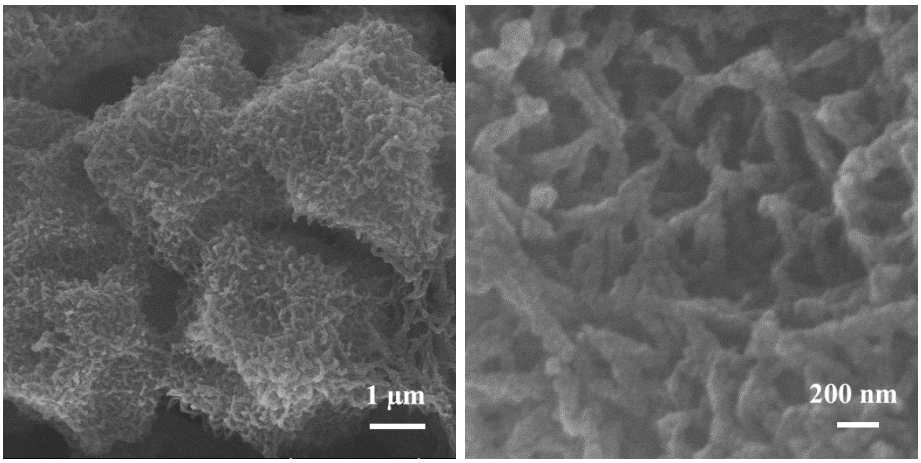

Fig. S5. SEM images of MOF-GC@$COF_{0.05}$.

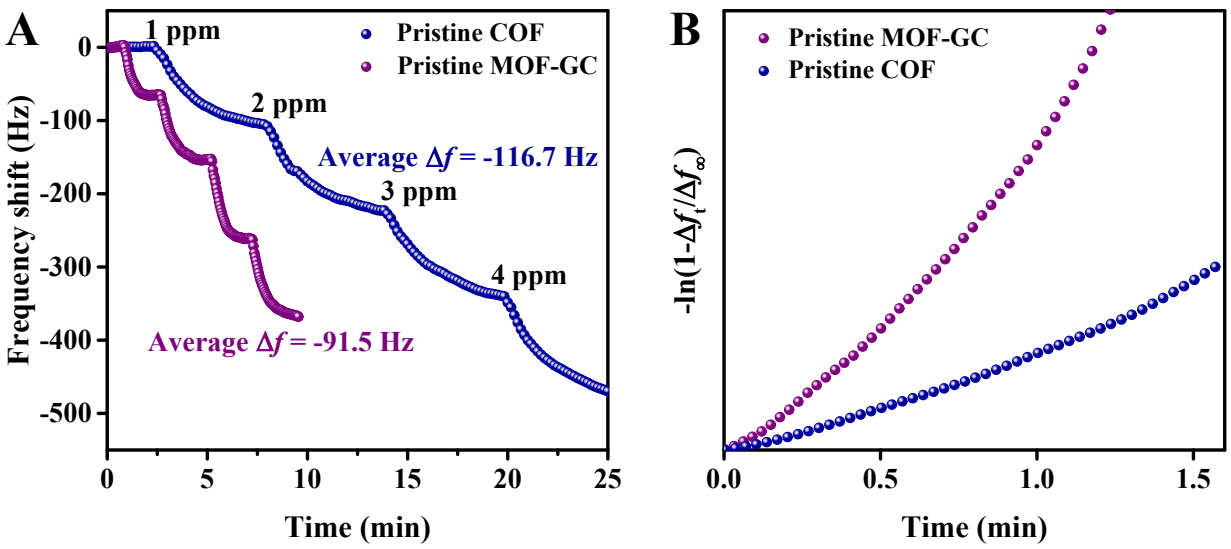

Fig. S6. (A) Real-time dynamic frequency shift curves of QCM sensors based on pristine MOF-GC and COF-TFP-DMPA on exposure to formaldehyde gas with increasing concentration from 1 to 4 ppm at room temperature. (B) Graphs of $-ln(1-\Delta f_t/\Delta f_\infty)$ against time t based on the pseudo-first-order kinetic model for the adsorption uptake of formaldehyde gas by pristine MOF-GC and COF-TFP-DMPA sensors.

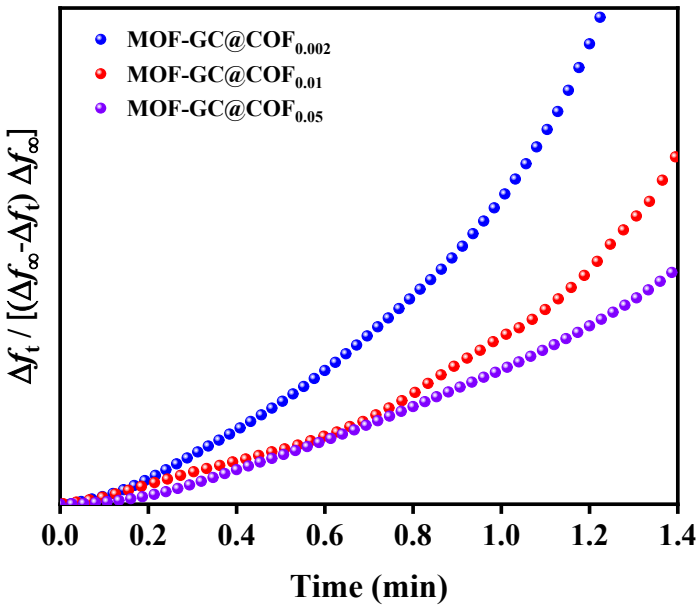

Fig. S7. Graphs of Δf_t /[(Δf_∞ -Δf_t) Δf_∞] against time *t* based on the pseudo-second-order kinetic model for the adsorption uptake of formaldehyde gas by MOF-GC@$COF_{0.002}$, MOF-GC@$COF_{0.01}$, and MOF-GC@$COF_{0.05}$ sensors.

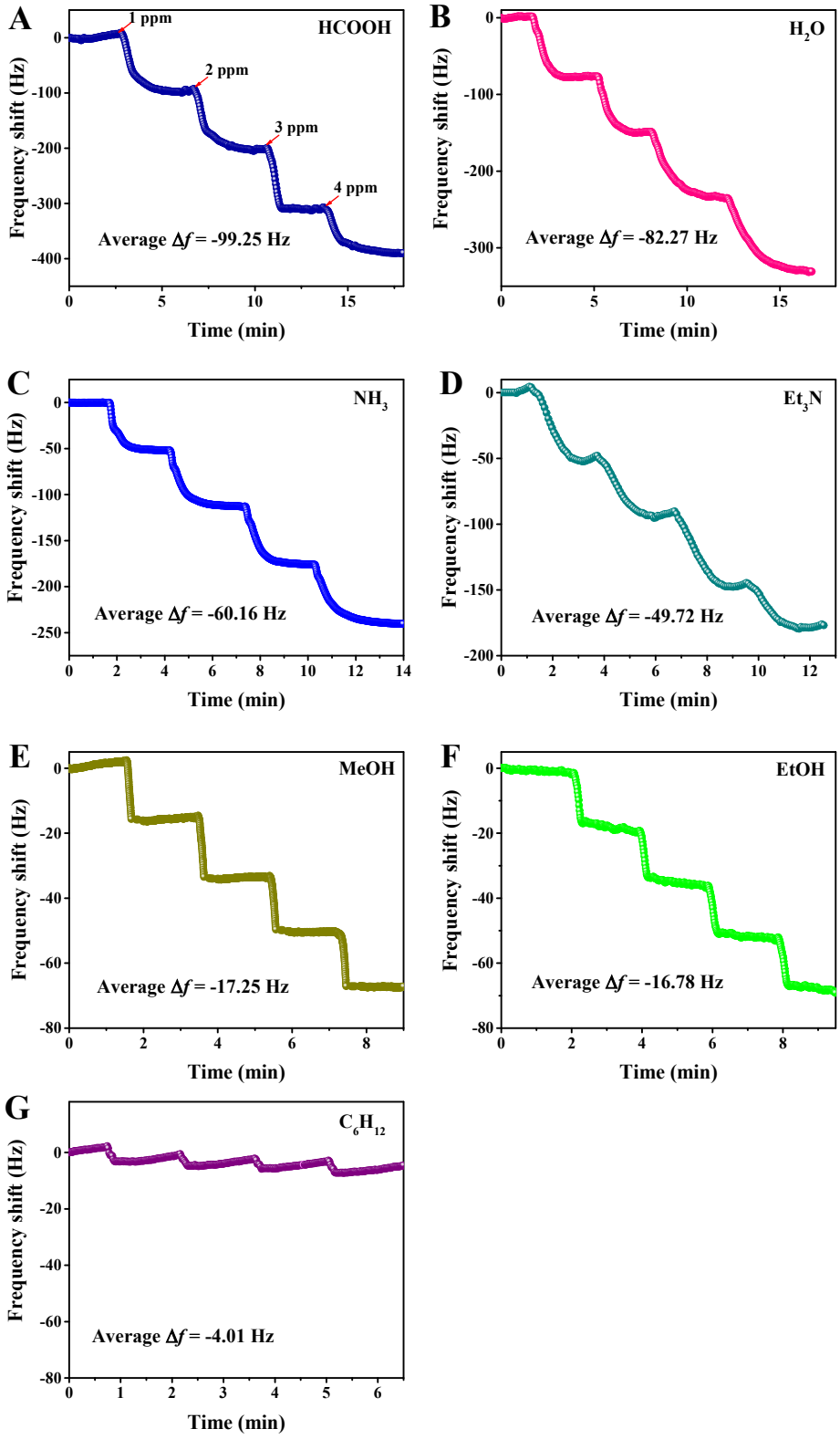

Fig. S8. Dynamic responses of QCM sensor based on MOF-GC@$COF_{0.01}$ on exposure to increasing concentration of different vapors at room temperature. (A) formic acid (HCOOH), (B) water (H_2O), (C) ammonia (NH_3), (D) triethylamine (Et_3N), (E) methanol (MeOH), (F) ethanol (EtOH), and (G) *n*-hexane (C_6H_{12}).

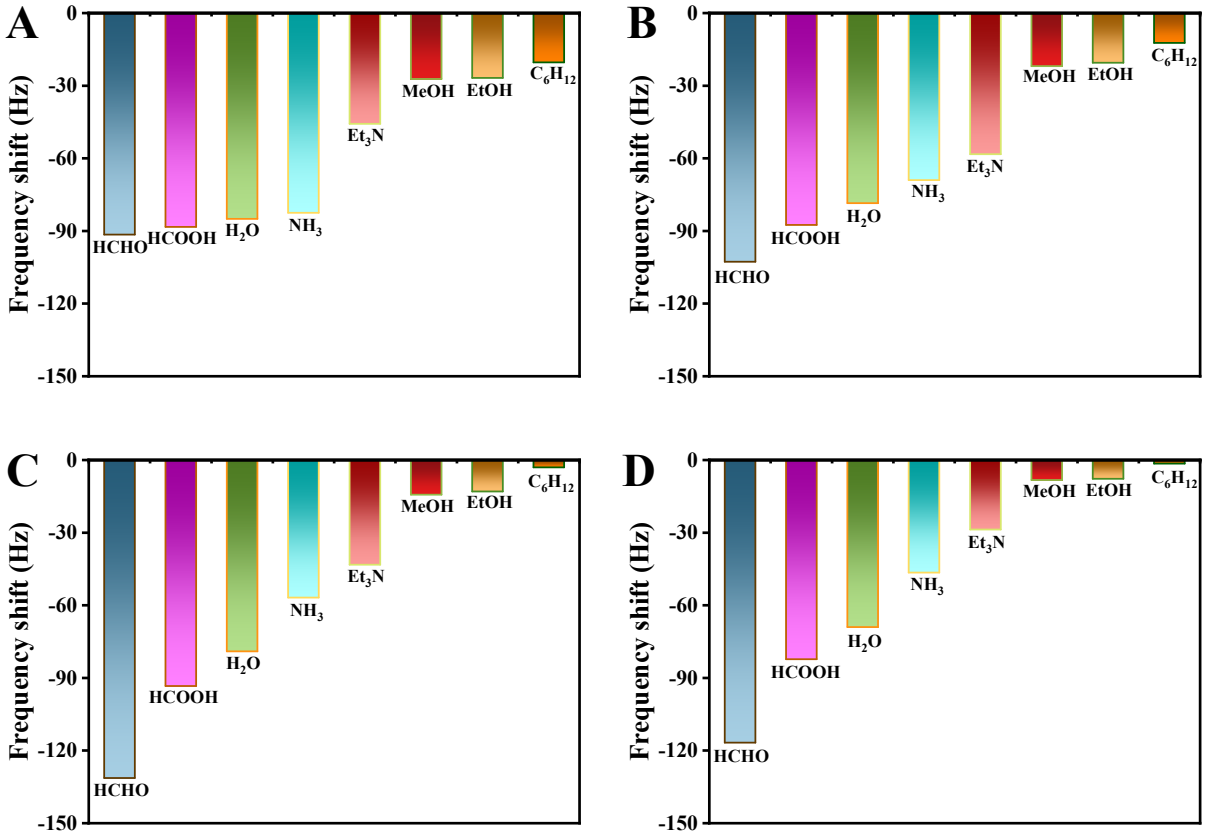

Fig. S9. The frequency shifts of QCM sensors based on pristine MOF-GC (A), MOF-GC@$COF_{0.002}$ (B), MOF-GC@$COF_{0.05}$ (C), and COF-TFP-DMPA (D) on exposure to different vapors at the concentration of 1 ppm, such as HCHO, HCOOH, H_2O, NH_3, Et_3N, MeOH, EtOH, and C_6H_{12}.

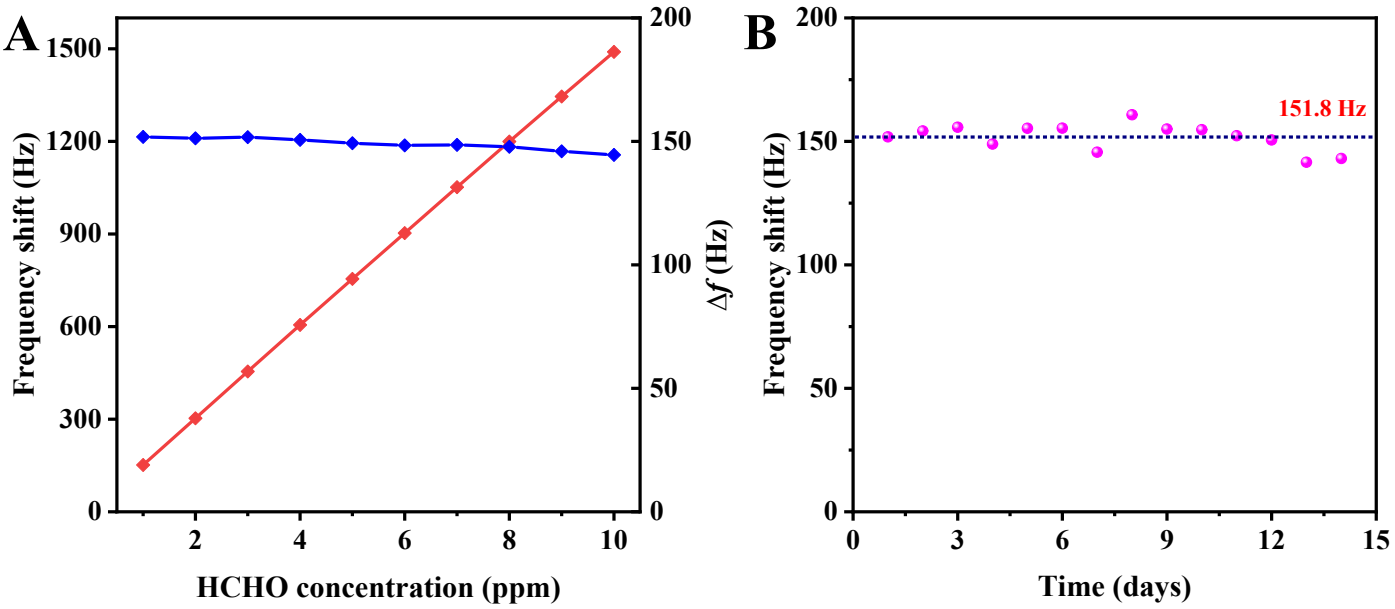

Figure S10. (A) Dynamic frequency shift (red) and Δf (blue) of the QCM sensor based on MOF-GC@$COF_{0.01}$ toward various concentrations of HCHO in a range of 1-10 ppm. (B) Long-term stability of the MOF-GC@$COF_{0.01}$ sensor to 1 ppm HCHO at room temperature.

References

[S1] C. Avci, J. Ariñez-Soriano, A. Carné-Sánchez, V. Guillerm, C. Carbonell, I. Imaz and D. Maspoch, *Angew. Chem. Int. Ed.*, 2015, **54**, 14417

[S2] a) M. Hu, J. Reboul, S. Furukawa, N. L. Torad, Q. Ji, P. Srinivasu, K. Ariga, S. Kitagawa and Y. Yamauchi, *J. Am. Chem. Soc*. 2012, **134**, 2864; b) N. L. Torad, H. Y. Lian, K. C. W. Wu, M. B. Zakaria, N. Suzuki, S. Ishihara, Q. Ji, M. Matsuura, K. Maekawa, K. Ariga, T. Kimura and Y. Yamauchi, *J. Mater. Chem.* 2012, **22**, 20008.

[S3] S. Zhang, J. Wang, N. L. Torad, W. Xia, M. A. Aslam, Y. V. Kaneti, Z. Hou, Z. Ding, B. Da, A. Fatehmulla, A. M. Aldhafiri, W. A. Farooq, J. Tang, Y. Bando and Y. Yamauchi, *Small*, 2020, **16**, 1901718.

[S4] X. Wang, B. Ding, M. Sun, J. Yu and G. Sun, *Sen. Actuators B*, 2010, **144**, 11.

[S5] C. Zhang, X. Wang, J. Lin, B. Ding, J. Yu and N. Pan, *Sen. Actuators B*, 2011, **152**, 316.

[S6] W. Hu, S. Chen, L. Liu, B. Ding, and H. Wang, *Sen. Actuators B*, 2011, 157, 554.

[S7] B. Ding, X. Wang, J. Yu and M. Wang, *J. Mater. Chem.*, 2011, **21**, 12784.

[S8] X. Wang, F. Cui, J. Lin, B. Ding, J. Yu and S. S. Al-Deyab, *Sen. Actuators B*, 2012,**171-172**, 658.

[S9] W. Huang, X. Wang, Y. Jia, X. Li, Z. Zhu, Y. Li, Y. Si, B. Ding, X. Wang and J. Yu, *RSC Adv.*, 2013, **3**, 22994.

[S10] L. Wang, Z. Wang, Q. Xiang, Y. Chen, Z. Duan and J. Xu, *Sen. Actuators B*, 2017, **248**, 820.

[S11] D. Yan, P. Xu, Q. Xiang, H. Mou, J. Xu, W. Wen, X. Li and Y. Zhang, *J. Mater. Chem. A*, 2016, **4**, 3487.

[S12] L. Wang, Y. Yu, Q. Xiang, J. Xu, Z. Chen and J. Xu, *Sen. Actuators B*, 2018, **255**, 2704.

[S13] J. Zong, Y. S. Zhang, Y. Zhu, Y. Zhao, W. Zhang and Y. Zhu, *Sen. Actuators B*, 2018, **271**, 311.

[S14] L. Wang, Y. Zhu, Q. Xiang, Z. Cheng, Y. Chen and J. Xu, *Sen. Actuators B*, 2017, **251**, 590.

[S15] Y. Zhu, H. Li, Y. Zhao, Q. Zheng, J. Xu and X. Li, *Langmuir*, 2012, **28**, 7843.